Crystal Structure of Phenylmethanesulfonyl Fluoride-Treated Human Chymase at 1.9 Å†

Mary E. McGrath,* Tara Mirzadegan,‡ and Brian F. Schmidt§

Arris Pharmaceutical, 385 Oyster Point Boulevard, Suite 3, South San Francisco, California 94080

Received June 11, 1997; Revised Manuscript Received September 9, 1997⊗

ABSTRACT: The X-ray crystal structure of human chymase has been determined to 1.9 Å resolution using molecular replacement methods. This first structure of human chymase is present as the Ser 195 ester of α-toluenesulfonic acid. The refined structure ($R_{cryst} = 0.183$) shows that the inhibitor phenyl moiety lies at the top of the major specificity pocket, S1, while the sulfur is covalently linked to Ser 195-Oγ. The sulfonyl oxygens interact with the oxyanion hole and with His 57-Nδ1. The presence of the inhibitor disturbs the usual *gauche* position of His 57 and forces it to the *trans* conformer. Though the primary binding pockets are similarly specific in chymase and chymotrypsin, examination of the extended substrate binding sites reveals the structural basis for chymase's greater discrimination in choosing substrates. The larger 30s loop and its proximity to the active site indicates that it contacts substrate residues C-terminal to the scissile bond. Modeling of substrate at the chymase active site suggests that binding energy may be gained by three main-chain hydrogen bonds provided by substrate residues P2′ and P4′ and that discriminating interactions with substrate side chains are also likely. The presence of Lys 40 in S1′ of human chymase explains its preference for Asp/Glu at P1′. Moreover, the cationic nature of S1′ provides a structural basis for human chymase's poor catalytic efficiency when angiotensin II is the substrate.

Only one chymase is believed to exist in humans, but it has been implicated in a number of important physiological processes. Chymase is known to be synthesized by mast cells as an inactive precursor, which is then stored in secretory granules. There it is packaged with heparin and processed by DPP1 (Murakami et al., 1995; Urata et al., 1993). The presence of mobile mast cells on the skin, in the heart, and in a number of other physiological niches places chymase at the scene of many processes in which it is thought to play a role. Activation of mast cells by cross-linking of the IgE on their surface or by the action of proteins such as C3a or C5a causes the elaboration of a number of cytokines, proteases, and other molecules that bring about acute biological responses. It is chymase itself, though, which has been characterized as important in inflammation (Bromley et al., 1984), hormone processing (Le Trong et al., 1987), and submucosal gland secretion (Sommerhof et al., 1989). In some instances, such as the activation of matrix metalloprotease 1 (MMP-1) (Saarinen et al., 1994) and the conversion of angiotensin I (AngI) to angiotensin II (AngII) (Urata et al., 1990), chymase has been shown to process its substrates in an exquisitely precise manner. This is contrasted with chymases of most other mammalian species, which are less specific and, for example, will proteolytically destroy AngII once they have made it (Le Trong et al., 1987).

The diversity of putative natural substrates and roles for human chymase, coupled with its striking resemblance to the nonspecific digestive enzyme chymotrypsin, make this an interesting molecule for structural study. Chymase and chymotrypsin share the same primary specificity for Phe, Tyr, Trp, and Leu. What structural features, then, provide chymase with its precision?

EXPERIMENTAL PROCEDURES

The covalent complex resulting from treatment of chymase with phenylmethanesulfonyl fluoride (PMSF) was prepared and crystallized as described (McGrath et al., 1997). Two crystal forms had been characterized, where the first is *C*2, with three or four molecules per asymmetric unit, while the second is $P2_12_12_1$ with no local symmetry. Though reasonably complete and high-resolution data sets were collected and analyzed for both crystal forms, only the orthorhombic crystal form has been solved at this time (Table 1). A 1.9 Å data set was collected from a single crystal of orthorhombic chymase−PMSF using a R-AXIS IV image plate system (MSC, The Woodlands, TX), equipped with focusing mirrors and a 0.001-in. nickel filter. The Biotex package (MSC, The Woodlands, TX) was utilized for data reduction. Software packages were implemented on a Silicon Graphics (Mountain View, CA) Indigo 2 workstation with Extreme Graphics.

The structure was solved by molecular replacement, using a homology construct (Homology, MSI, Inc.) of human chymase as the search model. Fabrication of the model was facilitated by similarity of chymase not only to chymotrypsin but also to rat mast cell protease II, for which a high-resolution X-ray structure is available (Remington et al., 1988). The grid-locked rotation function of the Xsight Module in Insight (MSI, Inc.) successfully generated a rotation solution when the search model of approximate dimensions 52 Å × 45 Å × 43 Å was placed in a triclinic

† Coordinates deposited with the Brookhaven Protein Data Bank as 1KLT.

* Corresponding author: telephone (415) 829-1154; Fax (415) 829-1123; email mcgrath@arris.com.

‡Present address: Roche Bioscience, Inc., 3401 Hillview Ave., Palo Alto, CA 94303.

§ Present address: Fibrogen, Inc., 260 Littlefield Ave., South San Francisco, CA 94080.

⊗ Abstract published in *Advance ACS Abstracts,* November 1, 1997.

S0006-2960(97)01403-7 CCC: $14.00

Table 1: Crystallographic Data for PMSF-Treated Chymase

space group	$P2_12_12_1$
cell dimensions (Å)	$a = 43.93$, $b = 58.16$, $c = 86.09$
R-AXIS IV	
resolution (Å)	1.9
data reduction package	Biotex (MSC)
no. of observations	31 632
no. of independent reflections	14 518
overall completeness to 1.9 Å (%)	84
% completeness 1.9 Å shell	50
no. of crystals	1
R_{merge}[a]	0.077
structure determination	molecular replacement using Xsight (Biosym/MSI)
model	homology model of chymase using Homology (MSI, Inc.)
refinement	X-PLOR
resolution range (Å)	6−1.9
no. of reflections used	14 003
no. of protein atoms	2137
no. of ordered waters	219
no. of inhibitor molecules	1
R_{cryst}[b]	0.183
R_{free}[c]	0.255
rms deviations	
bonds (Å)	0.016
angles (deg)	2.27
dihedrals (deg)	25.2
impropers (deg)	1.84

[a] $R_{merge} = \sum_h\sum_i|I_{h,i} - I_h|/\sum_h\sum_i I_{h,i}$, where I_h is the mean intensity of symmetry-related reflections, $I_{h,i}$. [b] $R_{cryst} = \sum||F_o| - |F_c||/\sum|F_o|$, where F_o and F_c are the observed and calculated structure factor amplitudes, respectively. [c] R_{free} is calculated the same as R_{cryst} but is for 10% of the data that is withheld from refinement.

box where all sides were 80 Å, and the included data was the 10−4 Å shell with a radius of 25 Å. The resultant 7.7σ peak (second highest signal was 4.2σ) was subjected to fine searching. The optimized solution produced a 11.6σ peak in the translation search. Subsequent examination of the packing of this putative cell revealed only minimal side-chain interactions between symmetry-related molecules.

Structure refinement in X-PLOR (Brünger, 1992b) (MSI, Inc.) commenced with treatment of the chymase molecule as a rigid group, which lowered the crystallographic residual from 47% to 44%. Subsequent positional and temperature factor refinement quickly reduced R_{cryst} to 25%. Additional refinement included simulated annealing, and rebuilding of several areas including residues 36−41, 168−174, and the C terminus. The structure was built using the Xsight Protein Crystal Structure Determination software (Biosym/MSI, San Diego, CA), which features the XtalView (McRee, 1993) routines for map visualization and electron density fitting. All data were used for map calculations. Crystallographic waters were located and added to the PDB file using the automatic water location routine which is part of this package. Criteria for acceptance of these water peaks were height greater than 2.6σ and distance of less than 3.4 Å from any solute atom, followed by visual inspection of each peak. Waters were deleted if their temperature factors exceeded 65 Å^2 after refinement. The final R_{cryst} is 18.3% with good geometry (Table 1). Cross validation (Brünger, 1992a), in which 10% of the data were excluded from refinement, was used to assess the suitability of refinement strategies, and the final R_{free} is 25.5%. Coordinates have been deposited with the Brookhaven Protein Data Bank as 1KLT.

For comparisons with related proteases and protease−inhibitor complexes, superpositioning of atomic coordinate sets was carried out using conserved core residues (see Figure 1). Structures used for the various analyses are the following: 1bit, trypsin (Smalas & Hordvik, 1993); 1acb, α-chymotrypsin complexed with eglin C (Bolognesi et al., 1992); 1cho, α-chymotrypsin complexed with turkey ovomucoid third domain (OMTKY3)(Fujinaga et al., 1987); 3rp2, rat mast cell protease II (Remington et al., 1988); 1hgt, thrombin (Skrzypczak-Jankun et al., 1991); 1hcg, factor Xa (Padmanabhan et al., 1993), and ecotin bound to rat anionic trypsin (McGrath et al., 1994).

The nomenclature of Schechter and Berger (1967) is used, in which substrate residues are described as P2, P1, P1′, etc., where P1 is the amino acid after which the peptide bond is cleaved, and P2 and P1′ flank P1 to the N- and C-terminal sides, respectively. Complementary binding sites on the protease are referred to as S2, S1, S1′, etc.

RESULTS AND DISCUSSION

Overall. As expected for a member of the chymotrypsin serine protease family, human chymase consists of two six-stranded β barrel domains that flank the active site. Superpositioning of the conserved core residues of the related proteases using 124 α-carbon positions produces rms deviations of 0.67 and 0.40 Å, for human chymase compared with α-chymotrypsin and rat mast cell protease II, respectively (Figure 1). Chymase shares primary structure identity on the order of 36% with chymotrypsin and 61% with rat mast cell protease II. Another related protease of interest is cathepsin G, which is 52% identical with chymase. The high-resolution structure of cathepsin G has been solved (Hof et al., 1996), but the coordinates were not available for comparison.

Chymase has been numbered in accordance with the paradigm, chymotrypsin. In this scheme the N-terminal amino acid of the mature protein is 16, signifying that the proregion of the zymogen is absent, and the enzyme ends with residue 245. In order to align these two proteases, insertions into the chymotrypsin sequence of residues 36a−c, 178a, and 186a,b are necessary, while residues 62, 149, 170−171, 203−206, and 222−223 are missing. All main-chain atoms of chymase are well-defined by electron density. The following side chains are not adequately represented by the data and so remain as alanines in the final coordinate set: Lys 109, Arg 137, Lys 186b, and Asn 245. These are all well away from the active site and thus the ambiguity of the surface side-chain positions is not likely to influence any of the conclusions stated in this paper.

Mature chymase commences with the N-terminus tucked into a binding pocket that is juxtaposed with the S1 specificity pocket. Here, as in related proteases, a salt bridge (2.7 Å) is formed between Ile 16 NH and Asn 194 Oδ2. While a hydrogen-bonding network purported to stabilize the zymogen extends into the protein from this point in the pancreatic proteases, no such network is evident in chymase. Proximal to this area, there are a number of lysines and arginines that form a region of positive charge on the chymase surface near the primary specificity pocket and activation cleft. These residues are arginines 137, 143, 161, 186a, and 188 and lysines 148 and 159. The existence of such a region was revealed by modeling studies and

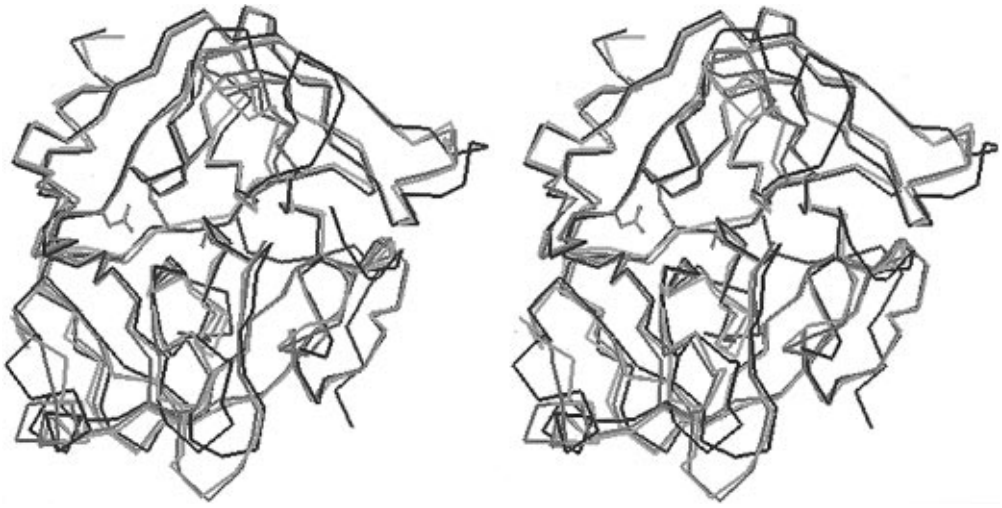

FIGURE 1: α-carbon traces are shown, in stereo, for chymotrypsin (blue), rat mast cell protease II (green), and human chymase (red) after superpositioning. This alignment was based on the following 124 "core" residues: 16−33, 42−59, 64−70, 80−123, 134−143, 153−164, 193−200, and 210−216. Various arrangements of core residues had been examined in order to obtain optimal superpositioning. Side-chain atoms are shown for the chymase catalytic triad Asp 102, His 57, and Ser 195. When the globular proteins are viewed as a clock face, the triad extends from 9:00 to the center, while the S1 specificity pocket would correspond to the center point extending out to 6:00. The 30s loops can be seen from 12:00 (mast cell proteases) to 1:00 (chymotrypsin).

postulated to be involved with heparin binding (Sali et al., 1993) and with stabilization of the N terminus before activation of the zymogen (Murakami et al., 1995). A similar concentration of positive charge is noted for cathepsin G (Hof et al., 1996).

The calcium binding loop (residues 70−80) of the digestive and clotting serine proteases has a non-metal-binding homologue in the leukocyte enzymes. Cathepsin G, granzymes, and kallikreins have Gln at position 80. The structure of cathepsin G (Hof et al., 1996) shows how this residue's side chain extends into the calcium-binding site and mimics the metal interactions by use of the terminal polar group. Human, baboon, dog, and mouse chymases appear to be an exception to this group of proteases in that they have Trp 80. In chymase, the Trp 80 side chain is tucked tightly into the binding site (Figure 2). π bonding interactions are possible between the backbone amides of Glu 77 and His 71 and ring atoms of Trp 80. However, seven close contacts (< 3.5 Å) are also evident. The electron density is strong and continuous for all residues in this region.

Catalytic Triad. Treatment of chymase with PMSF resulted in the esterification of Ser 195 with α-toluenesulfonic acid. The conformation of Ser 195 has not been significantly disturbed by this adduct, and the inhibitor sulfur lies 1.6 Å from Ser 195 Oγ. One sulfonyl oxygen is found in a hydrogen bond (3.1 Å) with a component of the oxyanion hole, Gly 193 NH (Figure 3). The other oxygen forms a bond with His 57. Binding of this inhibitor has caused a significant change in the side-chain position of His 57. The most frequently seen conformation for histidines in proteins deposited in the PDB (Bernstein et al., 1977) has been found to be *gauche*$^-$, followed by *trans*, with *gauche*$^+$ being least frequently observed (Sprang et al., 1987). The chymotrypsin-like serine proteases feature a *gauche*$^+$ conformer (where χ1 is approximately 90°) for His 57. This unusual rotamer appears to be stabilized by interactions with Asp 102 and Ser 195 (Sprang et al., 1987). In this chymase structure, His 57 is present as the *trans* rotamer, with a χ1 of −176°. This position avoids any unfavorable interactions with the inhibitor sulfonyl moiety and is very similar to that

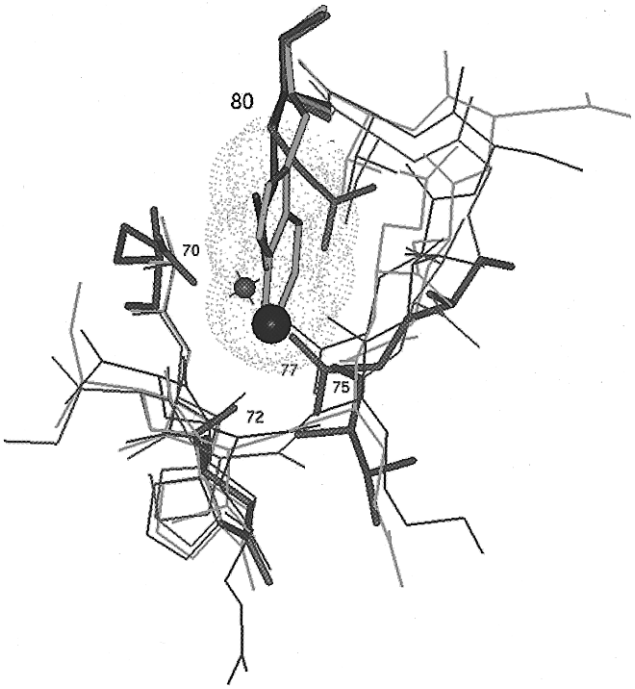

FIGURE 2: Calcium binding loops are shown for trypsin (purple), RMCPII (green), and chymase (red). The molecules were superimposed for this view using backbone atoms for the catalytic triad residues 57, 102 , and 195 and loop residues 70 and 80. Calcium is represented as a blue sphere, and its ligands, residues 70, 72, 75, 77, and 80, and one H_2O are rendered as thick lines and a sphere, respectively, for the trypsin structure. Calcium binding is not possible in the mast cell enzymes, which instead fill the site with side chains of loop residues. Gln 80 fills the site in RMCPII, while in chymase Trp 80 fits snugly into the loop, as shown by the van der Waals surface representation.

found for His 57 in other perturbed active sites: the structure of the Asp 102 to Asn mutant of rat trypsin has a *trans* His 57 (Sprang et al., 1987), as does the metal switch trypsin mutant in the presence of bound copper (McGrath et al., 1993). It seems that steric crowding, unfavorable hydrogen-bonding patterns, and the lure of interaction with bound metal are all sufficient to induce rotation of this histidine to a more frequently observed rotamer. This conformer of His 57 is

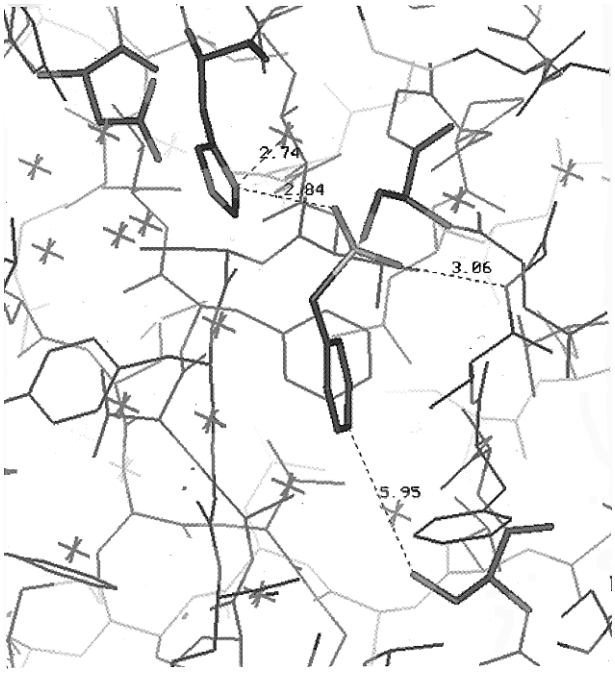

FIGURE 3: Interactions of α-toluenesulfonic acid with the chymase active site are shown. Atoms are colored by type, and the inhibitor and the catalytic triad His 57, Asp 102, and Ser 195 are rendered as sticks. Distances shown include minimal distance from the inhibitor phenyl ring to the base of the S1 specificity pocket and interactions made by the inhibitor sulfonyl group with His 57 and part of the oxyanion hole.

unable to bind to either the unavailable Ser 195 or Asp 102 but does interact with a sulfonyl oxygen as described above. It is most likely that His 57 Nδ1 and not Nϵ2 forms this bond, since the χ1 rotation from *gauche* to *trans* brings Nδ1 proximal to the inhibitor sulfonyl. This rotation of His 57 into solvent leaves a hole that is filled in both chymase and the metal switch trypsin mutant by a water molecule positioned to form a hydrogen bond with the His 57 imidazole. Asp 102 is equivalent to that found in other well-refined chymotrypsin-like structures. The structure shows that one side-chain oxygen bonds with His 57 NH, while the other bonds with Ser 214 Oγ and a water molecule.

Proximal to Asp 102, a water-filled channel links Ser 214 and the surface-accessible Tyr 234. Three waters mediate this distance, and all are within hydrogen-bonding distance of each other or the two bracketing protein residues (2.7, 3.0, 2.4, and 2.8 Å). This channel has been described for several of the chymotrypsin family proteases and implicated as being mechanistically significant (Meyer, 1992). It is better organized in chymase than in most related enzymes such as trypsin, chymotrypsin, and rat mast cell protease II, in which only two waters are present.

Specificity Pockets: (A) S1. The phenylmethane moiety of the inhibitor lies at the mouth of the S1 specificity pocket. At its closest point, it is 6 Å from the base of the pocket (Figure 3). Only very minimal binding energy could be derived from the limited number of possible van der Waals interactions that are observed at this site: the few contacts with the phenyl ring atoms involve Phe 191, Val 213, and Gly 216, while the methyl group of the PMSF is 3.6 Å from Ser 214 O. Thus, the phenylmethane group is not representative or predictive of a P1−S1 interaction. This main specificity pocket does contain two water molecules: one is bound to Ser 189 Oγ and Ala 190 O, and the other contacts the carbonyl oxygens of Pro 225 and Lys 221 and the backbone amide of Arg 217.

The S1 pocket bears a strong resemblance to chymotrypsin but is more related to RMCPII. Ser 189 forms the base of the pocket for chymotrypsin and chymase, while RMCPII has Ala 189. Chymotrypsin has Ser 190 while chymase and RMCPII have Ala at this site. At the base of the strand that forms the front of the S1 pocket, both chymase and RMCPII have a deletion of two residues compared with chymotrypsin. The deletion is flanked by two prolines, one of which, Pro 225, is found in the *cis* orientation. The strand that lies below and somewhat behind this segment has an insertion of two residues, 186a,b, relative to chymotrypsin. The most striking difference in S1 is the absence of the disulfide bond at Cys 191−Cys 220. Comparable to RMCPII and cathepsin G, Phe 191 is present, while small amino acids at position 220 (either Gly or Ala) facilitate the β turn from residues 220 to 223. In general, the chymase primary specificity pocket is large and uncharged, and its preference for Phe and Leu in the natural substrates AngI (Urata et al., 1990) and MMP-I (Saarinen et al., 1994), respectively, is not surprising.

Where chymotrypsin and the other digestive proteases exhibit selectivity almost exclusively through the P1−S1 interaction, the mast cell proteases show more stringent specificities derived from sites flanking P1 (Woodbury & Neurath, 1981). Modeling was used to examine putative interactions between substrates and the extended binding site of chymase. Coordinates for complexes of chymotrypsin [1acb (Bolognesi et al., 1992); 1cho(Fujinaga et al., 1987)] and trypsin [ecotin−trypsin (McGrath et al., 1994)] bound to macromolecular inhibitors were optimally superimposed onto chymase. Potential interactions between chymase and these substratelike molecules could be investigated. Amino acids on the inhibitor were replaced to mimic putative substrates. This analysis allows a first approximation of chymase−substrate interactions but is limited by inherent errors in modeling and by necessarily studying ground-state interactions. For example, though the sites are examined individually, kinetic evidence indicates that synergistic behavior between the subsites occurs. Furthermore, comparison of a series of acyl tetrapeptides showed that efficient hydrolysis of peptides containing the AngI P4−P1 sequence IleHisProPhe is due almost entirely to differences in k_{cat} (Sankar et al., 1997). Consequently, the energetic advantage afforded by this sequence is not available upon initial binding (or apparent by examination of a structural model of the ES complex) but is accessible in the transition state (Sankar et al., 1997).

(B) S2. Proline is often favored in the P2 position of chymotrypsin-like serine proteases, in part because it can tuck up near His 57 without steric hindrance, and also because it facilitates a change in direction of the substrate chain as it threads through the active site. Chymase also prefers Pro at P2, as demonstrated by the sequence of its substrate AngI and as determined using noncleavable peptide libraries (Bastos et al., 1995). The library work also indicated that Gln would be accommodated at P2. Chymase kinetic studies with nine tripeptide 4-nitroanilide substrates showed mostly small changes in k_{cat}/K_M when P2 was varied (Powers et al., 1985). However, Glu at P2 was, by far, the least reactive (16× lower than P2 Pro) (Powers et al., 1985). Modeling various amino acids at the chymase S2 pocket shows that placement of a Glu side chain at P2 would

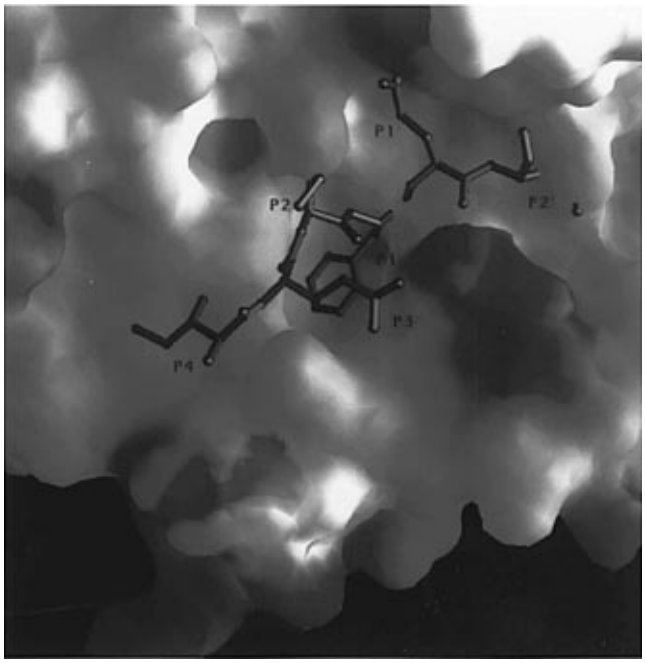

FIGURE 4: GRASP representation showing part of the reactive-site loop of mutated ecotin as it may interact with human chymase. The ecotin side chains have been replaced with those corresponding to a hypothetical chymase substrate, where P4 = Ile, P3 = Glu, P2 = Pro, P1 = Phe, P1′ = Glu, and P2′ = Asp. Calculated electrostatic potential is contoured from −7.6 *kT*/e (red) to 11.9 *kT*/e (blue). The concentration of negative charge just left of the P2 label corresponds to Asp 102 of the catalytic triad.

unfavorably juxtapose its negative charge (ca. 3.5 Å) with the significant negative potential (Figure 4) originating at Asp 102. Not surprisingly, Glu was a poor P2 substrate for the other related serine proteases tested in this study (Powers et al., 1985).

(C) S3. Chymotrypsin has no strong preferences at the P3 position, and examination of this site shows an absence of binding determinants. The leukocyte proteases appear to have features in this region that provide enhanced specificity. Modeling studies on RMCPII indicated that a P3 Phe would be well accommodated by a hydrophobic pocket in this region (Remington et al., 1988), while the P3 Val present at the active site of cathepsin G shows the side chain in a weak interaction with Lys 192 and Ser 218 (Hof et al., 1996). Chymase also has Lys and Ser at these positions and appears to prefer His (angiotensin I) and Glu [peptide library studies (Bastos et al., 1995)]. Experiments using tripeptide substrates indicated that Val was most preferred at P3 for human chymase but that Glu was almost as reactive (Powers et al., 1985). Modeling of these side chains shows that they could interact with Lys 192.

An interesting comparison can be made between the S3 specificity pockets of human and rat chymases. While both enzymes will convert AngI to AngII, the latter protease is less discriminating and will degrade (and thereby inactivate) AngII. Arg is at P3 when AngII is a substrate and would be repelled by Lys 192 in the binding pocket of chymase from both species. However, while Ser 218 forms a protrusion that guides the P3 side chain closer to Lys 192 in the human enzyme (Figure 4), Gly 218 in rat chymase would allow Arg to rotate away from Lys 192, which may make it an acceptable substrate.

(D) S4. The aryl binding pocket has been well-documented for some of the serine proteases involved in coagulation (Brandstetter et al., 1996; Stubbs et al., 1992). In human chymase this site is defined by Tyr 215, Phe 172, and the methylene side-chain atoms of Arg 217. Leu 99, Arg 173, and His 171 may also contribute interactions depending on the P4 residue. The site is clearly less organized and more open (Figure 4) than that seen in factor Xa (Padmanabhan et al., 1993), for example, where a hydrophobic channel is delimited by Tyr 99 and Phe 174. A P4 Ile, as present in AngI, would fit well at this site. The lack of binding determinants in this region explains why studies with tetrapeptide substrates varying at P4 showed only a 4-fold difference in affinity between the most and least reactive substrates (Powers et al., 1985). A small increase in k_{cat}/K_M was noted upon going from tri- to tetrapeptide substrates. Thus, the P4−S4 interaction should not be disregarded for the mast cell proteases.

(E) S1′. When the structures of chymotrypsin and chymase are compared, the most striking difference (Figure 1) is also one that strongly influences binding of residues C-terminal to the scissile bond. Chymase has an insertion of three residues, 36a−c (part of the 30s loop), relative to chymotrypsin. An insertion of two or three residues at this site is common for the granzymes, chymases, and cathepsin G. However, a change of direction of the polypeptide chain, compared to chymotrypsin, has at least as profound an effect as the inserted residues. In all these enzymes, this loop and the neighboring 60s loop are stabilized by the Cys 42−Cys 58 disulfide (Figure 5). The 40s strand, which is an integral part of one β barrel, continues straight out toward the surface for chymase and RMCPII but veers away from the active site for chymotrypsin (Figure 5). The deviation is such that the α carbons of the superimposed proteases are separated by 1 Å at position 34 but are approximately 6 Å apart by residue 36. In the mast cell proteases the strand continues out over the active site such that it forms the single largest protrusion from the surface of this globular protein (Figure 5). The strand rejoins that of chymotrypsin at residue 41. Again, the change in direction is so drastic that while the α carbons of residue 40 are 6 Å apart, the separation is only 1 Å at residue 41. In addition, the side chain of chymotrypsin Phe 41 is buried within the protein, while Phe 41 of chymase faces out where it would be proximal to a P2′ side chain.

The pocket that binds the P1′ residue is formed by the 60s and 30s loops. The 60s loop can be a site of variability in the chymotrypsin-like serine proteases, giving rise to substrate and inhibitor discrimination. For example, thrombin has an insertion of nine residues at this site and is refractory to inhibition by a number of macromolecular protease inhibitors because of steric clashes. The loop in chymase is mostly similar to that in chymotrysin, because while there is a deletion in chymase, it is positioned at residue 62, which is distal to S1′. Furthermore, the constancy of His 57 and Cys 58 throughout many members of this family limits the differences between the enzymes in this region. Interestingly, the lack of major binding determinants in the 60s region may be compensated for by the unusual position of the 30s loop in chymase, which, at its terminus, approaches the position seen for the extended 60s loop in factor Xa (Figure 5).

Peptide inhibitor library studies (Bastos et al., 1995) showed that chymase prefers Glu and Asp at P1′, while the natural substrates AngI and MMP-I have P1′ His and Thr, respectively. This chymase structure indicates that the

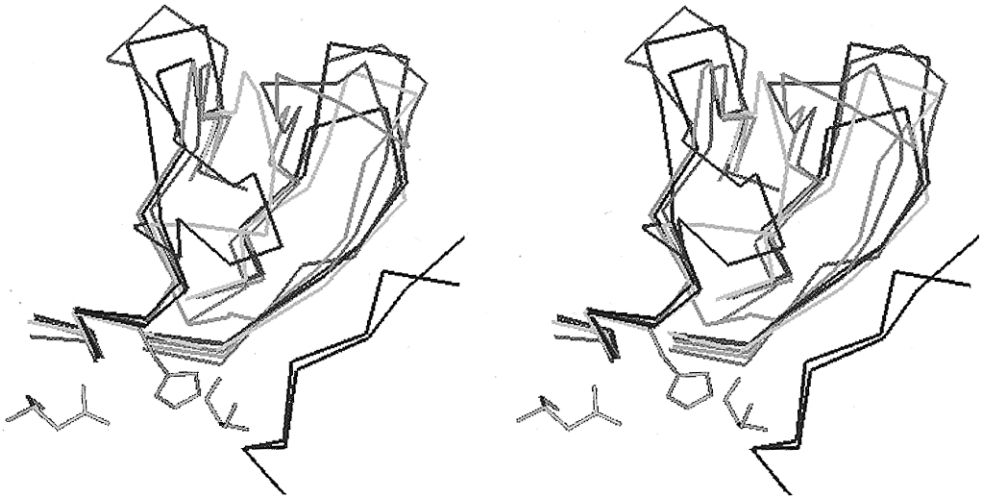

FIGURE 5: α-Carbon traces of the 60s and 30s loops are shown for a number of the chymotrypsin family serine proteases (superimposed by core residues) in stereo. The 60s loop is on the left, where His 57 of the catalytic triad can be seen at the bottom, flanked by Asp 102 and Ser 195. The conserved disulfide bond Cys 42−Cys 58 is also shown for chymase. To the right of the 60s loop is the 30s loop. In addition, heptapeptides of the inhibitors ecotin and BPTI are shown as they bind at the active sites of trypsin and chymotrypsin, respectively. The coloring scheme is as follows: red = chymase; black = trypsin−ecotin; blue = chymotrypsin−OMTKY3; yellow = factor Xa; purple = thrombin; green = RMCPII. The large 60s loop in thrombin precludes binding of some proteinaceous inhibitors, while a smaller insertion in factor Xa is not as sterically limiting. Residue 36 and 36a in chymase and RMCPII lie approximately 3 Å from the 60s loop of factor Xa (Ala 61A).

driving force for these interactions is S1′ component Lys 40, which appears to be able to contact Glu, Asp, or His at P1′ (Figure 4). His 57 O can also contact the P1′ side chain and would be able to bond with a substrate Thr at this site. Val 40 in RMCPII would dictate a very different specificity at P1′.

Mammalian chymases, other than those of human and baboon, are able to hydrolyze (and thus destroy the biological activity of) AngII. These enzymes likely owe part of their more relaxed specificity to the nondiscriminatory Ala at position 40. A recent study (Sankar et al., 1997) compared the relative catalytic efficiencies for human and rat chymases for the Phe^8−His^9 bond (which is cleaved to make AngII) versus the Tyr^4−Ile^5 bond (which is cleaved to destroy AngII). Human chymase cleaves the Phe^8−His^9 bond with a 780-fold greater catalytic efficiency than the Tyr^4−Ile^5 bond. The authors conclude that synergistic interactions of binding subsites are responsible for the low hydrolytic rate of human chymase toward Tyr-Ile and state that a substrate P1′ Ile is nonoptimal for human chymase. Our structure shows that the presence of Lys 40 in S1′ would discourage binding of Ile. This single interaction may play a significant role in protecting AngII from hydrolysis in man. However, as demonstrated by Sankar et al. (1997), mutually dependent interactions between the subsites appear to modulate substrate binding and behavior in the transition state. Such phenomena are not readily deconvoluted by examination of substrate modeled into an enzyme active site. The P1′−residue 40 interaction is not possible in chymotrypsin and related enzymes in which the 30s loop does not approach the active site. Thus, it would appear that the more discriminating serine proteases, such as those of the clotting cascade and elaborated from mast cells, can use the juxtaposed 60s and 30s loops to limit substrates.

(F) S2′−S4′. It is likely that chymase obtains binding energy and exhibits greater specificity than chymotrypsin partly due to interactions beyond P1′. Crystal structures of a number of substrate and inhibitor complexes involving chymotrypsin-like serine proteases have shown that antiparallel main-chain hydrogen bonding between P2-P3 and the protease is present and is a source of considerable binding energy (Bode & Huber, 1992). In a comparable manner, but at the other side of the scissile bond, residues 39−41 of chymase run antiparallel to modeled substrate, providing the potential for three hydrogen bonds (3.4, 3.2, and 3.3 Å) to be formed with carbonyls and amides of P2′ and P4′ (Figure 6). (No effort has been made to optimize these somewhat long potential hydrogen bonds.) In agreement with our modeling results, peptide substrate studies indicate that, C-terminal to the scissile bond, significant binding energy is derived from main-chain interactions. Placement of Gly at P1′−P3′ in the context of an AngI analogue resulted in a 2.5-fold higher k_{cat}/K_M than that measured for the natural

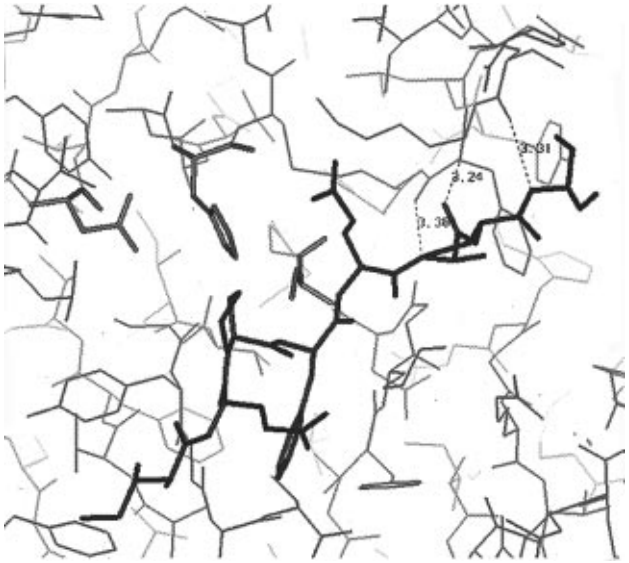

FIGURE 6: The inhibitor ecotin, with side chains replaced to complement chymase specificity, is shown modeled at the human chymase active site. The possibility of antiparallel main-chain hydrogen bonding between chymase and the primed side of the substrate is shown. No attempt has been made to optimize these distances by torsioning of atoms.

P1′-P2′ dipeptide in the same peptide framework (Sankar et al., 1997). Thus, the positively charged side chain of Lys 40 in human chymase may exert its influence more by dissuading inappropriate substrates at P1′ than by reaping binding energy with optimal substrates. Inhibitor library studies (Bastos et al., 1995) did show preferences for particular side chains and indicated that chymase prefers Asp and Glu at P2′. These side chains may interact with the appropriately placed Arg 143 of chymase. While P3′ faces solvent and is probably not important for substrate selection, the proximity of chymase Ser 39 may provide some discrimination at P4′. Thus, the 30s loop in chymase, and probably in the related RMCPII and cathepsin G, is a significant source of binding energy and bears responsibility for substrate discernment from P1′ to P4′.

To conclude, human chymase displays exquisite sensitivity towards its biological substrates while bearing a remarkable resemblance to the relatively nondiscriminatory chymotrypsin. Whereas the related coagulation enzymes limit their substrates by modification of the 60s loop and the S4 aryl binding site, this new structure suggests that specialization of chymase is partly derived from determinants C-terminal to the scissile peptide bond. We observe once again how the small changes that distinguish these highly related enzymes have profound biological consequences.

ACKNOWLEDGMENT

We thank Drs. Brad Katz, Jim Clark, and Jeff Spencer for helpful discussions.

REFERENCES

Bastos, M., Maeji, N. J., & Abeles, R. H. (1995) *Proc. Natl. Acad. Sci. U.S.A. 92*, 6738−6742.

Bernstein, F. C., Koetzle, T. F., Williams, G. J. B., Meyer, E. F., Brice, M. D., Rodgers, J. R., Kennard, O., Shimanouchi, T., & Tasumi, M. (1977) *J. Mol. Biol. 112*, 535−542.

Bode, W., & Huber, R. (1992) *Eur. J. Biochem. 204*, 433−451.

Bolognesi, M., Frigerio, F., Coda, A., Pugliese, L., Lionetti, C., Menegatti, E., Amiconi, G., Schnebli, H. P., & Ascenzi, P. (1992) *J. Mol. Biol. 225*, 107.

Brandstetter, H., Kühne, A., Bode, W., Huber, R., von der Saal, W., Wirthensohn, K., & Engh, R. A. (1996) *J. Biol. Chem. 271*, 29988−29992.

Bromley, M., Fisher, W. D., & Woolley, D. E. (1984) *Ann. Rheum. Dis. 43*, 76−79.

Brünger, A. T. (1992a) *Nature 355*, 472.

Brünger, A. T. (1992b) *X-PLOR Version 3.1 Manual*, Yale University Press, New Haven, CT, and London.

Fujinaga, M., Sielecki, A. R., Read, R. J., Ardelt, W., Laskowski, M., Jr., & James, M. N. G. (1987) *J. Mol. Biol. 195*, 397−418.

Hof, P., Mayr, I., Huber, R., Korzus, E., Potempa, J., Travis, J., Powers, J., & Bode, W. (1996) *EMBO J. 15*, 5481−5491.

Le Trong, H., Neurath, H., & Woodbury, R. G. (1987) *Proc. Natl. Acad. Sci. U.S.A. 84*, 364−367.

McGrath, M. E., Haymore, B. L., Summers, N. L., Craik, C. S., & Fletterick, R. J. (1993) *Biochemistry 32*, 1914−1919.

McGrath, M. E., Engel, T., Bystroff, C., & Fletterick, R. J. (1994) *EMBO J. 13*, 1502−1507.

McGrath, M. E., Osawa, A. E., Barnes, M. G., Clark, J. M., Mortara, K. D., & Schmidt, B. F. (1997) *FEBS Lett. 413*, 486−488.

McRee, D. E. (1993) *Practical Protein Crystallography*, Academic Press, New York.

Meyer, E. (1992) *Protein Sci. 1*, 1543−1562.

Murakami, M., Karnik, S., & Husain, A. (1995) *J. Biol. Chem. 270*, 2218−2223.

Padmanabhan, K., Padmanabhan, K. P., Tulinsky, A., Park, C. H., Bode, W., Huber, R., Blankenship, D. T., Cardin, A. D., & Kisiel, W. (1993) *J. Mol. Biol. 232*, 947−967.

Powers, J. C., Tanaka, T., Harper, J. W., Minematsu, Y., Barker, L., Lincoln, D., Crumley, K. V., Fraki, J. E., Schechter, N. M., Lazarus, G. G., Nakajima, K., Nakashino, K., Neurath, H., & Woodbury, R. G. (1985) *Biochemistry 24*, 2048−2058.

Remington, S. J., Woodbury, R. G., Reynolds, R. A., Matthews, B. W., & Neurath, H. (1988) *Biochemistry 27*, 8097.

Saarinen, J., Kalkkinen, N., Welgus, H. G., & Kovanen, P. T. (1994) *J. Biol. Chem. 269*, 18134−18140.

Sali, A., Matsumoto, R., McNeil, H. P., Karplus, M., & Stevens, R. L. (1993) *J. Biol. Chem. 268*, 9023−9034.

Sankar, S., Chandrasekharan, U., Wilk, D., Glynias, M. J., Karnik, S. S., & Husain, A. (1997) *J. Biol. Chem. 272*, 2963−2968.

Schechter, I., & Berger, A. (1967) *Biochem. Biophys. Res. Commun. 27*, 157−162.

Skrzypczak-Jankun, E., Carperos, V. E., Ravichandran, K. G., Tulinsky, A., Westbrook, M., & Maraganore, J. M. (1991) *J. Mol. Biol. 221*, 1379.

Smalas, A. O., & Hordvik, A. (1993) *Acta Crystallogr., Sect. D 49*, 318.

Sommerhof, C. P., Caughey, G. H., Finkbeiner, W. E., Lazarus, S. C., Basbaum, C. B., & Nadel, J. A. (1989) *J. Immunol. 142*, 2450−2456.

Sprang, S., Standing, T., Fletterick, R. J., Stroud, R. M., Finer-Moore, J., Xuong, N.-H., Hamlin, R., Rutter, W. J., & Craik, C. S. (1987) *Science 237*, 905−909.

Stubbs, M., Oschkinat, H., Mayr, I., Huber, R., Angliker, H., Stone, S., & Bode, W. (1992) *Eur. J. Biochem. 206*, 187−195.

Urata, H., Kinoshita, A., Misono, K. S., Bumpus, F. M., & Husain, A. (1990) *J. Biol. Chem. 265*, 22348−22357.

Urata, H., Karnik, S., Graham, R., & Husain, A. (1993) *J. Biol. Chem. 268*, 24318−24322.

Woodbury, R. G., & Neurath, H. (1981) in *Metabolic Interconversion of Enzymes* (Holzer, H., Ed.) p 145, Springer-Verlag, Berlin.

BI971403N